Hindawi Publishing Corporation
Mathematical Problems in Engineering
Volume 2009, Article ID 526945, 16 pages
doi:10.1155/2009/526945

Review Article

Flow Around a Slender Circular Cylinder: A Case Study on Distributed Hopf Bifurcation

J. A. P. Aranha, K. P. Burr, I. C. Barbeiro, I. Korkischko, and J. R. Meneghini

Nucleus of Dynamics and Fluids (NDF), Mechanical Engineering, University of Sao Paulo, Sao Paulo, Brazil

Correspondence should be addressed to J. A. P. Aranha, japaran@usp.br

Received 17 December 2008; Accepted 6 January 2009

Recommended by José Roberto Castilho Piqueira

This paper presents a short overview of the flow around a slender circular cylinder, the purpose being to place it within the frame of the distributed Hopf bifurcation problems described by the Ginzburg-Landau equation (GLE). In particular, the chaotic behavior superposed to a well tuned harmonic oscillation observed in the range Re > 270, with Re being the Reynolds number, is related to the defect-chaos regime of the GLE. Apparently new results, related to a Kolmogorov like length scale and the *rms* of the response amplitude, are derived in this defect-chaos regime and further related to the experimental *rms* of the lift coefficient measured in the range Re > 270.

1. Flow Around a Circular Cylinder: An Overview

Let a cylinder with a circular cross section in the plane $\mathbf{x} = (x, y)$ exposed to an incident flow $U\mathbf{i}$; if d is the circle diameter and ν the kinematic fluid viscosity, the Reynolds number is defined by $\mathrm{Re} = Ud/\nu$. Assuming a unit system where $\rho = U = d = 1$, with ρ being the fluid density, the two-dimensional (2D) velocity and pressure fields, respectively $\{\mathbf{u}(\mathbf{x}, t); p(\mathbf{x}, t)\}$, satisfy the Navier-Stokes equations,

$$\begin{aligned} &\frac{\partial \mathbf{u}}{\partial t} + (\mathbf{u} \cdot \nabla)\mathbf{u} - \frac{1}{\mathrm{Re}}\nabla^2\mathbf{u} + \nabla p = \mathbf{0}; \\ &\nabla \cdot \mathbf{u} = 0, \quad \left(\nabla = \mathbf{i}\frac{\partial}{\partial x} + \mathbf{j}\frac{\partial}{\partial y}\right), \end{aligned} \tag{1.1}$$

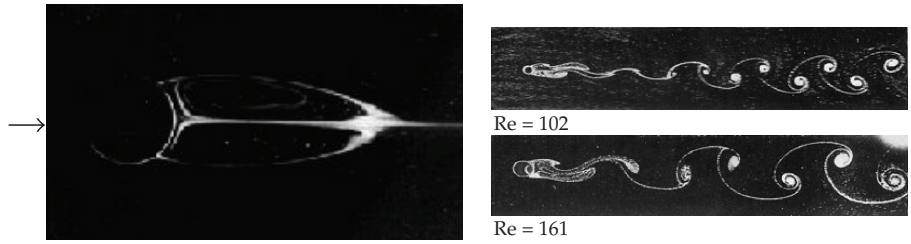

Figure 1: Flow around circular cylinder: (a) *steady state regime*, Re = 40 < 46.5; (b) *stable 2D limit cycles*, 46.5 < Re < 180 (Re = 102 above, Re = 161, below). (source: Van Dyke [1]).

and the boundary conditions (∂V_c: cylinder cross section)

$$\begin{aligned} \mathbf{u}(\mathbf{x},t)\big|_{\mathbf{x}\in\partial V_c} &= \mathbf{0}; \\ \lim_{\|\mathbf{x}\|\to\infty} \{\mathbf{u}(\mathbf{x},t); p(\mathbf{x},t)\} &= \{U\mathbf{i}; 0\}. \end{aligned} \tag{1.2}$$

Equations (1.1) and (1.2) has a *steady solution* $\mathbf{u}_s(\mathbf{x})$ that is however *stable* only in the range Re < 46.5; for Re > 46.5 a *limit cycle solution*, oscillating with the *Strouhal frequency* $\omega_s \approx U/d$, is observed. This limit cycle is stable in the 2D context—namely, if the perturbation is restricted to the plane $\mathbf{x} = (x, y)$—in a large range of Reynolds numbers and Figure 1 shows typical flow visualizations in the steady (Re = 40) and limit cycles regimes (Re = 102;161).

The periodic flow in the limit cycle regime can be expanded in its harmonic components by Fourier series decomposition; namely, if $\mathbf{u}(\mathbf{x},t) = u(\mathbf{x},t)\mathbf{i} + v(\mathbf{x},t)\mathbf{j}$ is the flow field then

$$\begin{aligned} u(\mathbf{x},t) &= u_o(\mathbf{x}) + \sum_{n=1}^{\infty} \left[u_{n,c}(\mathbf{x}) \cdot \cos(n\omega_s t) + u_{n,s}(\mathbf{x}) \cdot \sin(n\omega_s t)\right]; \\ v(\mathbf{x},t) &= v_o(\mathbf{x}) + \sum_{n=1}^{\infty} \left[v_{n,c}(\mathbf{x}) \cdot \cos(n\omega_s t) + v_{n,s}(\mathbf{x}) \cdot \sin(n\omega_s t)\right]. \end{aligned} \tag{1.3}$$

The time average $\mathbf{u}_o(\mathbf{x}) = u_o(\mathbf{x})\mathbf{i} + v_o(\mathbf{x})\mathbf{j}$ of $\mathbf{u}(\mathbf{x},t)$ is a flow field *symmetric* with respect to the x-axis, with $u_o(\mathbf{x})$ being an *even* function of $y(u_o(x,y) = u_o(x,-y))$ and $v_o(\mathbf{x})$ an *odd* one $(v_o(x,y) = -v_o(x,-y))$; the first harmonic $\mathbf{u}_1(\mathbf{x}) = u_1(\mathbf{x})\mathbf{i} + v_1(\mathbf{x})\mathbf{j}$ is an *anti-symmetric* field, with $\{u_1(x,y) = -u_1(x,-y); v_1(x,y) = v_1(x,-y)\}$ and, as a rule, one can show for a circular cylinder that the even harmonics are symmetric and the odd ones anti-symmetric: the *in-line force* (drag) depends thus only on the *even modes* while the *transverse force* (lift) depends only on the *odd modes*. Figure 2 displays, for Re = 100, the functions $\{(u_{1,c}(\mathbf{x}), v_{1,c}(\mathbf{x})); (u_{2,c}(\mathbf{x}), v_{2,c}(\mathbf{x}))\}$ obtained both from numerical simulation of the 2D flow and from PIV measurement of an actual flow experiment. Both plots are visually very similar and confirm the symmetry/anti-symmetry behavior quoted above; furthermore, the agreement between them is also quantitative: defining the *normalized mode amplitude* by the ratio $A_n(\mathrm{Re}) = \max|u_n(\mathbf{x})|/\max|u_o(\mathbf{x})|$, Figure 3 displays the function $A_n(\mathrm{Re})$ determined numerically in the range $60 \le \mathrm{Re} \le 600$ and also the same value obtained experimentally at Re = 100.

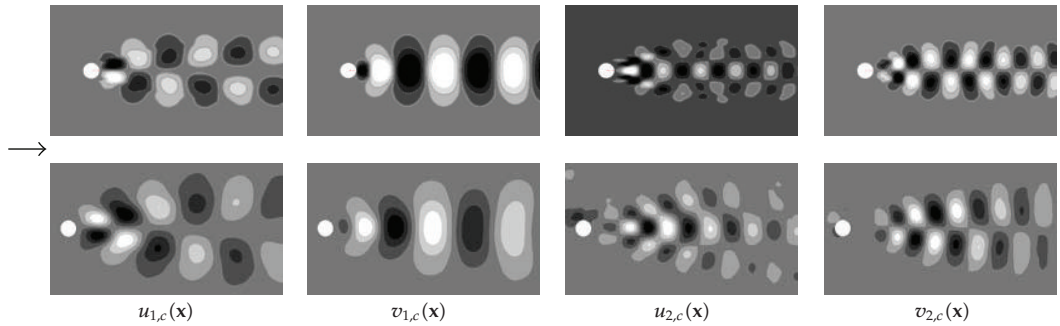

Figure 2: Harmonic decomposition of the 2D velocity field—Re = 100. *Above:* numerical simulation; *below:* experiments (PIV). (Source: Barbeiro & Korkischko (2008)—NDF).

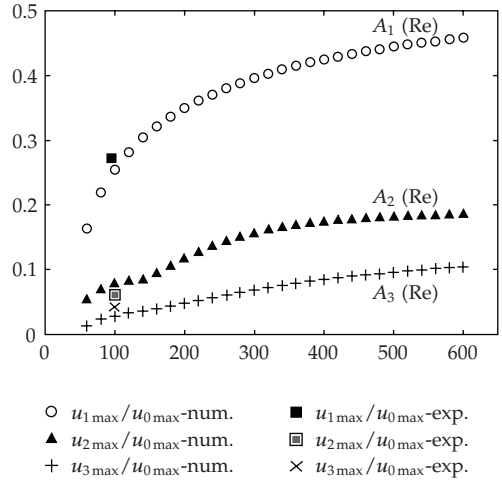

Figure 3: Amplitude $A_n(\mathrm{Re}) = = \max|u_n(\mathbf{x})|/\max|u_o(\mathbf{x})|$ of the nth mode. Numerical computation (for Re = 100, also shown PIV computation) (source: Barbeiro & Korkischko (2008)—NDF).

It must be observed also that these numerical results indicate a *hierarchy* between the modes amplitudes and a *square root singularity* near $\mathbf{R}_{c1} \cong 46.5$, namely

$$\begin{gathered} A_n(\mathrm{Re}) \cong \mathcal{O}(\varepsilon^n); \\ A_1(\mathrm{Re}) \cong \mathcal{O}(\varepsilon) \quad \text{with } \varepsilon(\mathrm{Re}) \cong 0.45\sqrt{1 - \frac{\mathbf{R}_{c1}}{\mathrm{Re}}}, \end{gathered} \tag{1.4}$$

typical of a *Hopf supercritical bifurcation*. This point will be elaborated in the following; in fact, if one writes (1.3) in the complex form,

$$\begin{gathered} \mathbf{u}_n(\mathbf{x}) = \frac{1}{2}\left(\mathbf{u}_{n,c}(\mathbf{x}) - i\mathbf{u}_{n,s}(\mathbf{x})\right); \\ \mathbf{u}(\mathbf{x},t) = \mathbf{u}_o(\mathbf{x}) + \sum_{n=1}^{\infty}\left(\mathbf{u}_n(\mathbf{x}) \cdot \mathbf{e}^{\mathrm{in}\omega_s t} + (*)\right), \quad \left(\lim_{\|\mathbf{x}\|\to\infty} \left\{ \begin{array}{l} \mathbf{u}_o(\mathbf{x}) \\ \mathbf{u}_n(\mathbf{x});\ n > 0 \end{array} \right\} = \left\{ \begin{array}{c} U\mathbf{i} \\ \mathbf{0} \end{array} \right\}\right), \end{gathered} \tag{1.5}$$

placing (1.5) into (1.1) and separating the harmonic parcels $\{\exp(in\omega_s t);\ n = 0,1,2,\ldots\}$ one obtains the sequence of problems,

$$\begin{aligned}
&\mathbf{n} = \mathbf{0} : (\mathbf{u}_o \cdot \nabla)\mathbf{u}_o - \frac{1}{\mathrm{Re}}\nabla^2\mathbf{u}_o + \nabla p_o = \mathbf{f}_o(\mathbf{x}) \\
&\quad = -\sum_{n=1}^{\infty}\left[(\mathbf{u}_n \cdot \nabla)\mathbf{u}_n^* + (\mathbf{u}_n^* \cdot \nabla)\mathbf{u}_n\right] \cong \mathcal{O}(\varepsilon^2); \\
&\mathbf{n} = \mathbf{1} : i\omega_s\mathbf{u}_1 + \left[(\mathbf{u}_o \cdot \nabla)\mathbf{u}_1 + (\mathbf{u}_1 \cdot \nabla)\mathbf{u}_o\right] - \frac{1}{\mathrm{Re}}\nabla^2\mathbf{u}_1 + \nabla p_1 = \mathbf{f}_1(\mathbf{x}) \\
&\quad = -\sum_{n=1}^{\infty}\left[(\mathbf{u}_{n+1} \cdot \nabla)\mathbf{u}_n^* + (\mathbf{u}_n^* \cdot \nabla)\mathbf{u}_{n+1}\right] \cong \mathcal{O}(\varepsilon^3); \\
&\mathbf{n} = \mathbf{2} : 2i\omega_s\mathbf{u}_2 + \left[(\mathbf{u}_o \cdot \nabla)\mathbf{u}_2 + (\mathbf{u}_2 \cdot \nabla)\mathbf{u}_o\right] - \frac{1}{\mathrm{Re}}\nabla^2\mathbf{u}_2 + \nabla p_2 = \mathbf{f}_2(\mathbf{x}) \\
&\quad = -(\mathbf{u}_1 \cdot \nabla)\mathbf{u}_1 - \sum_{n=1}^{\infty}\left[(\mathbf{u}_{n+2} \cdot \nabla)\mathbf{u}_n^* + (\mathbf{u}_n^* \cdot \nabla)\mathbf{u}_{n+2}\right] \cong \mathcal{O}(\varepsilon^2); \quad (\nabla \cdot \mathbf{u}_n = 0),
\end{aligned} \tag{1.6}$$

the first one, that determines $\mathbf{u}_o(\mathbf{x})$, being nonlinear and the remaining ones linear, as usual in an asymptotic expansion. In fact, if higher order terms in the "small parameter" ε are disregarded, one may express, to leading order, the field $\mathbf{u}_1(\mathbf{x})$ in the form

$$\begin{aligned}
&\mathbf{u}_1(\mathbf{x}) = a_{\mathrm{av}} \cdot \mathbf{e}_{\mathrm{av}}(\mathbf{x}) + \mathcal{O}(\varepsilon^3); \\
&i\omega_s\mathbf{e}_{\mathrm{av}} + \left[(\mathbf{u}_o \cdot \nabla)\mathbf{e}_{\mathrm{av}} + (\mathbf{e}_{\mathrm{av}} \cdot \nabla)\mathbf{u}_o\right] - \frac{1}{\mathrm{Re}}\nabla^2\mathbf{e}_{\mathrm{av}} + \nabla p_{\mathrm{av}} = \mathbf{0}, \quad (\nabla \cdot \mathbf{e}_{\mathrm{av}} = 0),
\end{aligned} \tag{1.7}$$

with $\{\lambda_{\mathrm{av}} = i\omega_s; \mathbf{e}_{\mathrm{av}}(\mathbf{x})\}$ being the eigenvalue—eigenvector of the homogeneous problem defined in (1.7): this is consistent with a numerical result due to Barkley [2], stating that the *averaged flow* $\mathbf{u}_o(\mathbf{x})$ is *marginally stable* (*Real* $\lambda_{\mathrm{av}} = 0$) with respect to 2D perturbation.

But this is not enough for the present purpose: the final goal is to solve the tridimensional (3D) problem for a *slender* cylinder having to solve basically the 2D cross section problem: besides the obvious economy in the degrees of freedom needed in the numerical computation, the 2D flow is well organized (*laminar*) while the 3D one is chaotic (*turbulent*), as it will be seen later in this paper. As discussed in Aranha [3], the flow around a slender cylinder can be asymptotically approximated by the *Ginzburg-Landau equation* but one needs then, first of all, to express the harmonic mode $\mathbf{u}_1(\mathbf{x}) \cdot \exp(i\omega_s t)$ in the form $a(t) \cdot \mathbf{e}(\mathbf{x})$, as in (1.7), with $a(t)$ satisfying *Landau's equation*

$$\begin{aligned}
&\frac{da}{dt} - \sigma a + \mu(1 - ic_3)|a|^2 a = 0; \\
&\varepsilon = \sqrt{\frac{\sigma}{\mu}}, \quad (\lambda = \sigma + i\omega).
\end{aligned} \tag{1.8}$$

The hope is that such $a(t) \cdot \mathbf{e}(\mathbf{x})$, with the related eigenvalue-eigenvector $\{\lambda(\mathrm{Re}) = \sigma + i\omega; \mathbf{e}(\mathbf{x}; \mathrm{Re})\}$, coalesce with the standard *Hopf bifurcation* in the limit $\varepsilon \to 0$ ($\mathrm{Re} \to \mathbf{R}_{c1}$), while

recovering the *Fourier series expansion* (1.5) when ε^2 is "small" but finite in the range $\mathrm{Re} \gg \mathbf{R}_{c1}$. This double requisite obliges to look for a *basic stationary flow* that is neither the *steady solution* $\mathbf{u}_s(\mathbf{x})$, useless far from the bifurcation, nor the *averaged flow* $\mathbf{u}_o(\mathbf{x})$, always marginally stable and so unsuited to describe a Hopf bifurcation.

A clue is given by the following observation: the *steady state solution* $\mathbf{u}_s(\mathbf{x};\mathrm{Re})$, that becomes unstable at $\mathrm{Re} = \mathbf{R}_{c1}$, satisfies the *homogeneous* 0th-order equation (1.6); with $\mathbf{f}_o(\mathbf{x})$ defined in (1.6), if one considers instead of $\mathbf{u}_s(\mathbf{x};\mathrm{Re})$ the field

$$\begin{aligned} &(\widehat{\mathbf{u}}_o \cdot \nabla)\widehat{\mathbf{u}}_o - \frac{1}{\mathrm{Re}}\nabla^2\widehat{\mathbf{u}}_o + \nabla\widehat{p}_o = \mathbf{f}_o(\mathbf{x};\mathrm{Re}) - \Delta\mathbf{f}_o(\mathbf{x};\mathrm{Re}) \cong \mathcal{O}(\varepsilon^4);\\ &\Delta\mathbf{f}_o(\mathbf{x};\mathrm{Re}) = -\left[(\mathbf{u}_1^* \cdot \nabla)\mathbf{u}_1 + (\mathbf{u}_1 \cdot \nabla)\mathbf{u}_1^*\right] \cong \mathcal{O}(\varepsilon^2), \quad (\widehat{\mathbf{u}}_o - \mathbf{u}_s \cong \mathcal{O}(\varepsilon^4)), \end{aligned} \tag{1.9}$$

the stability of this flow coalesce with the one related to the *steady state solution* $\mathbf{u}_s(\mathbf{x};\mathrm{Re})$ with an error of order ε^4 in the limit $\sigma \to 0$ $(\mathrm{Re} \to \mathbf{R}_{c1})$: in Hopf bifurcation one has $\sigma(\mathrm{Re}) = \alpha \cdot (1 - \mathbf{R}_{c1}/\mathrm{Re}) \approx \varepsilon^2$ when $\mathrm{Re} \to \mathbf{R}_{c1}$ and this relation is recovered if the field defined in (1.9) is used, instead of the standard steady state solution $\mathbf{u}_s(\mathbf{x};\mathrm{Re})$, as the basic field.

At $\mathbf{R}_{c1}$ one has strictly $\mathbf{u}_s(\mathbf{x};\mathbf{R}_{c1}) \equiv \mathbf{u}_o(\mathbf{x};\mathbf{R}_{c1})$; however, as Re increases the *steady state solution* $\mathbf{u}_s(\mathbf{x};\mathrm{Re})$ presents a bulbous region in the wake, similar to the one indicated in Figure 1 but with a length increasing linearly with Re: the difference between $\mathbf{u}_s(\mathbf{x};\mathrm{Re})$ and $\mathbf{u}_o(\mathbf{x};\mathrm{Re})$ becomes enormous in the range $\mathrm{Re} > 200$, in despite of the fact that the forcing term $\mathbf{f}_o(\mathbf{x})$ in the problem that defines $\mathbf{u}_o(\mathbf{x};\mathrm{Re})$ be small, of order ε^2. This apparent paradox is in fact due to an extreme susceptibility of the *steady flow* $\mathbf{u}_s(\mathbf{x};\mathrm{Re})$ to the influence of "small forces", either applied directly, as $\mathbf{f}_o(\mathbf{x})$, or else indirectly, as the constraint forces that appear on the outer contour of the finite domain used in the numerical computation; for example, to determine numerically $\mathbf{u}_s(\mathbf{x})$ at $\mathrm{Re} = 600$ with reasonable accuracy one needs to discretize a circle with radius $1000d$: only then the "small constraint forces" in the outer circle becomes small enough to not impair convergence. In the other hand, the presence of the small forcing term $\mathbf{f}_o(\mathbf{x})$ seems to regularize the problem, since then the *time average* field $\mathbf{u}_o(\mathbf{x};\mathrm{Re})$ is robust: it can be easily determined numerically, without any major concern about the region size to be discretized, and it also changes weakly with the Reynolds number.

In the asymptotic solution that leads to Landau's equation (1.8) terms of order ε^4 are ignored and the fields $\{\widehat{\mathbf{u}}_o;\widehat{p}_o\}$ can be thus determined by solving the *regular* linear system

$$\left.\begin{aligned} \widehat{\mathbf{u}}_o &= \mathbf{u}_o - \delta\mathbf{u};\\ \widehat{p}_o &= p_o - \delta p; \end{aligned}\right\} \Longrightarrow [(\mathbf{u}_o \cdot \nabla)\delta\mathbf{u} + (\delta\mathbf{u} \cdot \nabla)\mathbf{u}_o] - \frac{1}{\mathrm{Re}}\nabla^2(\delta\mathbf{u}) + \nabla(\delta p) = \Delta\mathbf{f}_o \cong \mathcal{O}(\varepsilon^2), \tag{1.10}$$

where the term $(\delta\mathbf{u} \cdot \nabla)\delta\mathbf{u} \cong \mathcal{O}(\varepsilon^4)$ was disregarded; notice that the linear operator (1.10) is *regular* since its eigenvalue λ with largest real part is given by $\{\mathrm{Real}\,\lambda = 0;\ \mathrm{Imag}\,\lambda = \omega_s \cong \mathcal{O}(1)\}$, see (1.7).

The eigenvalue-eigenvector $\{\lambda(\mathrm{Re}) = \sigma + i\omega;\ \mathbf{e}(\mathbf{x};\mathrm{Re})\}$ corresponding to the basic flow defined in (1.9) is solution of the problem

$$\begin{aligned} &\lambda\mathbf{e} + \left[(\widehat{\mathbf{u}}_o \cdot \nabla)\mathbf{e} + (\mathbf{e} \cdot \nabla)\widehat{\mathbf{u}}_o\right] - \frac{1}{\mathrm{Re}}\nabla^2\mathbf{e} + \nabla p_e = \mathbf{0};\\ &\lambda = \sigma + i\omega \quad \text{with } \sigma(\mathrm{Re}) > 0 \quad \text{if } \mathrm{Re} > \mathbf{R}_{c1}, \quad (\nabla \cdot \mathbf{e} = 0), \end{aligned} \tag{1.11}$$

and since $\{\widehat{\mathbf{u}}_o - \mathbf{u}_o; \widehat{p}_o - p_o\} \cong \mathcal{O}(\varepsilon^2)$, comparing (1.7) to (1.11) one obtains

$$\begin{gathered}\{\mathbf{e} - \mathbf{e}_{\mathrm{av}}; p_e - p_{\mathrm{av}}\} \cong \mathcal{O}(\varepsilon^2);\\ \sigma + i(\omega - \omega_s) \cong \mathcal{O}(\varepsilon^2).\end{gathered} \tag{1.12}$$

Observing that the harmonic components $\{\mathbf{u}_n(\mathbf{x}); n > 0\}$ in (1.5) tend to zero as $\|\mathbf{x}\| \to \infty$, and so it does the functions $\{\mathbf{f}_o(\mathbf{x}); \Delta\mathbf{f}_o(\mathbf{x})\}$, one considers now the solution of

$$\begin{gathered}\frac{\partial \widehat{\mathbf{u}}}{\partial t} + (\widehat{\mathbf{u}} \cdot \nabla)\widehat{\mathbf{u}} - \frac{1}{\mathrm{Re}}\nabla^2\widehat{\mathbf{u}} + \nabla\widehat{p} = \mathbf{f}_o(\mathbf{x}; \mathrm{Re}) - \Delta\mathbf{f}_o(\mathbf{x}; \mathrm{Re}) \cong \mathcal{O}(\varepsilon^4);\\ \nabla \cdot \widehat{\mathbf{u}} = 0,\end{gathered} \tag{1.13}$$

satisfying the same boundary conditions (1.2). The *steady state solution* of (1.13), defined in (1.9), becomes unstable for $\mathrm{Re} > \mathbf{R}_{c1}$, the only *unstable mode* being given by $\{\lambda(\mathrm{Re}) = \sigma + i\omega; \mathbf{e}(\mathbf{x}; \mathrm{Re})\}$, solution of (1.11); the solution of (1.13) in the unstable range $\mathrm{Re} > \mathbf{R}_{c1}$ can be thus expressed by means of the standard asymptotic series

$$\begin{aligned}\widehat{\mathbf{u}}(\mathbf{x}, t) &= \widehat{\mathbf{u}}_o(\mathbf{x}) + \left[a(t) \cdot \mathbf{e}(\mathbf{x})e^{i\omega t} + (*)\right] + \left[\left|a(t)\right|^2 \cdot \mathbf{u}_{20}(\mathbf{x}) + \left(a^2(t) \cdot \mathbf{u}_{22}(\mathbf{x})e^{2i\omega t} + (*)\right)\right]\\ &\quad + \left[\left|a(t)\right|^2 a(t) \cdot \mathbf{u}_{31}(\mathbf{x})e^{i\omega t} + a^3(t) \cdot \mathbf{u}_{33}(\mathbf{x})e^{3i\omega t}\right] + \mathcal{O}(\varepsilon^4);\\ \widehat{p}(\mathbf{x}, t) &= \widehat{p}_o(\mathbf{x}) + \left[a(t) \cdot p_e(\mathbf{x})e^{i\omega t} + (*)\right] + \left[\left|a(t)\right|^2 \cdot p_{20}(\mathbf{x}) + \left(a^2(t) \cdot p_{22}(\mathbf{x})e^{2i\omega t} + (*)\right)\right]\\ &\quad + \left[\left|a(t)\right|^2 a(t) \cdot p_{31}(\mathbf{x})e^{i\omega t} + a^3(t) \cdot p_{33}(\mathbf{x})e^{3i\omega t}\right] + \mathcal{O}(\varepsilon^4);\\ a &\cong \mathcal{O}(\varepsilon); \qquad \frac{da}{dt} \cong \mathcal{O}(\varepsilon^3); \qquad \left\{(\widehat{\mathbf{u}}_o, \widehat{p}_o); (\mathbf{e}, p_e); (\mathbf{u}_{\alpha\beta}, p_{\alpha\beta})\right\} \cong \mathcal{O}(1),\end{aligned} \tag{1.14}$$

where (*) stands for the complex conjugate of the expression in the left and, as usual, the *mode amplitude* $a(t)$ is assumed to change slowly in time, the slow time being proportional to the amplitude square.

By placing (1.14) into (1.13) and separating terms of like orders in ε, a sequence of *linear problems* is obtained, allowing to compute the fields $\{\mathbf{u}_{\alpha\beta}(\mathbf{x}); p_{\alpha\beta}(\mathbf{x})\}$. Details will be omitted here but two points must be commented. First, the operator that determines $\mathbf{u}_{31}(\mathbf{x})$ is exactly the one defined in (1.11) and it is thus singular: the solvability condition (*Fredholm alternative*) of this $\mathbf{u}_{31}$-equation leads to *Landau's equation* (1.8); second, for future reference, the field $\mathbf{u}_{20}(\mathbf{x})$ is solution of the equation

$$\begin{gathered}\left[(\mathbf{u}_o \cdot \nabla)\mathbf{u}_{20} + (\mathbf{u}_{20} \cdot \nabla)\mathbf{u}_o\right] - \frac{1}{\mathrm{Re}}\nabla^2\mathbf{u}_{20} + \nabla p_{20} = \mathbf{f}_{20};\\ \mathbf{f}_{20} = -\left[(\mathbf{e}^* \cdot \nabla)\mathbf{e} + (\mathbf{e} \cdot \nabla)\mathbf{e}^*\right],\end{gathered} \tag{1.15}$$

where the relation $(\widehat{\mathbf{u}}_o - \mathbf{u}_o) \cdot |a(t)|^2\mathbf{u}_{20} \cong \mathcal{O}(\varepsilon^4)$ was used.

The 2D systems (1.1) and (1.13) have both the same singularity at $\mathbf{R}_{c1} \cong 46.5$ and are both regular in "all range" $\mathrm{Re} > \mathbf{R}_{c1}$, a result numerically confirmed by Henderson [4] up

to Re = 1000; since one system differ from the other only by a forcing term of order ε^4, one should have asymptotically

$$\begin{aligned}\mathbf{u}(\mathbf{x},t) &= \widehat{\mathbf{u}}(\mathbf{x},t) + \mathcal{O}(\varepsilon^4);\\ p(\mathbf{x},t) &= \widehat{p}(\mathbf{x},t) + \mathcal{O}(\varepsilon^4),\end{aligned} \tag{1.16}$$

a result that will be explored next. In fact, recalling that $\{\widehat{\mathbf{u}}_o - \mathbf{u}_o; \widehat{p}_o - p_o\} \cong \mathcal{O}(\varepsilon^2)$ one has, with the help of (1.16),

$$\left.\begin{aligned}\mathbf{u}(\mathbf{x},t) &= \mathbf{u}_o(\mathbf{x}) + \left[\mathbf{u}_1(\mathbf{x})e^{i\omega_s t} + (*)\right] + \mathcal{O}(\varepsilon^2);\\ \widehat{\mathbf{u}}(\mathbf{x},t) &= \mathbf{u}_o(\mathbf{x}) + \left[a(t)\cdot\mathbf{e}(\mathbf{x})e^{i\omega t} + (*)\right] + \mathcal{O}(\varepsilon^2);\end{aligned}\right\} \Longrightarrow \mathbf{u}_1(\mathbf{x})e^{i\omega_s t} = a(t)\cdot\mathbf{e}(\mathbf{x})e^{i\omega t} + \mathcal{O}(\varepsilon^3). \tag{1.17}$$

Two results can be derived directly from the latter equality (see also (1.9) and (1.15)),

$$\begin{aligned}\left|a(t)\right|^2\mathbf{f}_{20}(\mathbf{x}) = \Delta\mathbf{f}_o(\mathbf{x}) + \mathcal{O}(\varepsilon^4) &\Longrightarrow \left|a(t)\right|^2\mathbf{u}_{20}(\mathbf{x}) = \delta\mathbf{u}(\mathbf{x}) + \mathcal{O}(\varepsilon^4);\\ a(t) &= |a|\cdot e^{i(\omega_s-\omega)t},\end{aligned} \tag{1.18}$$

and thus it follows from (1.14) that the asymptotic solution of (1.13), based on the *Landau's equation* (1.8), recovers the observed 2D periodic (limit cycle) solution (1.5) in the range $\mathrm{Re} \gg \mathbf{R}_{c1}$, with an error of order ε^4. Or in short: Landau's equation (1.8), strictly valid in a close neighborhood of a *Hopf supercritical bifurcation*, can be extended in the present flow problem to the range $\mathrm{Re} \gg \mathbf{R}_{c1}$, where a neat periodic solution persists.

Finally, once the 2D numerical solution $\mathbf{u}(\mathbf{x},t)$ is determined and its harmonic components $\{\mathbf{u}_n(\mathbf{x}); n = 0,1,2,3\}$ are computed, the *unstable mode* $\{\lambda = \sigma + i\omega; \mathbf{e}(\mathbf{x}); p_e(\mathbf{x})\}$ and the coefficients $\{\mu; c_3\}$ of *Landau's equation* can be easily estimated, as elaborated below. In fact, using the approximations and the normalization of the mode $\mathbf{e}(\mathbf{x})$,

$$\begin{aligned}\mathbf{e}(\mathbf{x}) &= \frac{\mathbf{u}_1(\mathbf{x})}{|a|} + \mathcal{O}(\varepsilon^2);\\ p_e(\mathbf{x}) &= \frac{p_1(\mathbf{x})}{|a|} + \mathcal{O}(\varepsilon^2);\\ \int_S ||\mathbf{e}(\mathbf{x})||^2 dS = 1 &\Longrightarrow |a| = \left(\int_S ||\mathbf{u}_1(\mathbf{x})||^2 dS\right)^{1/2} + \mathcal{O}(\varepsilon^2),\end{aligned} \tag{1.19}$$

multiplying (1.11) by $\mathbf{e}^*(\mathbf{x})$, integrating by parts and using $\nabla\cdot\mathbf{e}^* = 0$, one obtains

$$\lambda = \sigma + i\omega = -\int_S \left[(\widehat{\mathbf{u}}_o\cdot\nabla)\mathbf{e} + (\mathbf{e}\cdot\nabla)\widehat{\mathbf{u}}_o\right]\cdot\mathbf{e}^* dS - \frac{1}{\mathrm{Re}}\int_S (\nabla\mathbf{e} : \nabla\mathbf{e}^*) dS, \tag{1.20}$$

with $\nabla \mathbf{e} : \nabla \mathbf{e}^* = \nabla e_x \cdot \nabla e_x^* + \nabla e_y \cdot \nabla e_y^*$. Using again the approximation $\mathbf{e}_{\text{av}} \cong \mathbf{u}_1(\mathbf{x})/|a| \cong \mathbf{e}$, with the same error ε^2 in (1.7), the following identity can be derived,

$$i\omega_s = -\int_S \left[(\mathbf{u}_o \cdot \nabla)\mathbf{e} + (\mathbf{e} \cdot \nabla)\mathbf{u}_o\right] \cdot \mathbf{e}^* dS - \frac{1}{\text{Re}} \int_S (\nabla \mathbf{e} : \nabla \mathbf{e}^*) dS, \tag{1.21}$$

and subtracting one expression from the other, while using $\hat{\mathbf{u}}_o = \mathbf{u}_o - \delta\mathbf{u}$, one obtains

$$\sigma + i(\omega - \omega_s) \cong \int_S \left[(\delta\mathbf{u} \cdot \nabla)\mathbf{e} + (\mathbf{e} \cdot \nabla)\delta\mathbf{u}\right] \cdot \mathbf{e}^* dS, \tag{1.22}$$

with $\delta\mathbf{u}(\mathbf{x}; \text{Re}) \cong \mathcal{O}(\varepsilon^2)$ being solution of the regular linear system (1.10).

Notice that (1.22) reaffirms, as it should, the estimated orders in (1.12) and placing the $a(t)$ defined in (1.18) into Landau's equation (1.8) one has

$$\begin{aligned} \mu &\cong \frac{\sigma}{|a|^2}; \\ c_3 &\cong \frac{\omega_s - \omega}{\sigma}. \end{aligned} \tag{1.23}$$

Summarizing: through the 2D simulation one obtains $\{\mathbf{u}(\mathbf{x}, t); p(\mathbf{x}, t)\}$ and from the Fourier expansion in the harmonics of the observed frequency ω_s one determines the *averaged flow* $\{\mathbf{u}_o(\mathbf{x}; \text{Re}); p_o(\mathbf{x}; \text{Re})\}$ and the *first harmonic* $\{\mathbf{u}_1(\mathbf{x}; \text{Re}); p_1(\mathbf{x}; \text{Re})\}$ defined in (1.5). Solving the linear system (1.10) the field $\delta\mathbf{u}(\mathbf{x}; \text{Re})$ can be computed and so the coefficients of Landau's equation using (1.19), (1.22), and (1.23). The gain in this extra computation is certainly marginal in the context of the 2D problem; however, as it will be discussed in the following sections, Landau's equation is the basis of the 3D Ginzburg-Landau equation (GLE) and with it one can possible predict an asymptotic approximation of the 3D behavior without having to resort to a 3D numerical computation of the flow field. In this context, the proposed approximation is similar to existing "slender body theories" in applied mechanics, as for example the *Lifting Line Theory* in the Aerodynamics of slender wings: in all of them one takes profit of the body slenderness to correct asymptotically the 2D solution. But before one addresses this 3D extension of Landau's equation it is worth to mention some general features of the actual 3D flow around a slender cylinder.

2. Features of the 3D Flow Around a Slender Cylinder

The 2D flow around a slender 3D cylinder is *unstable* with respect to *3D-perturbation* for Re > 190 and this is instability, known experimentally for a long time, has only recently been verified theoretically in a comprehensive numerical study done by Henderson [4]. The plot of the Strouhal number $\text{St} = f_s d/U$ ($f_s = \omega_s/2\pi$) as a function of Re, see Figure 4, portrays this instability in a very clear way and Henderson [4] has shown that the bifurcation at $\mathbf{R}_{c2} \cong 190$ is *subcritical* while a second one at $\mathbf{R}_{c3} \cong 260$ is *supercritical*. The curve St(Re) presents a hysteretic behavior in the range $180 < \text{Re} \leq 260$, where two competing solutions, corresponding to two distinct attractors, can appear depending on the initial conditions; as

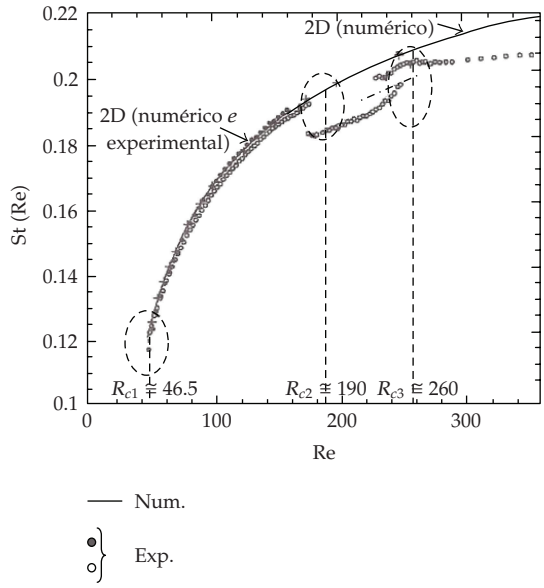

Figure 4: Strouhal number St = $f_s d/U (f_s = \omega_s/2\pi)$ as a function of Re. (Bifurcations points $\mathbf{R}_{C1}; \mathbf{R}_{C2}$ and $\mathbf{R}_{C3}$—source: Henderson [4].)

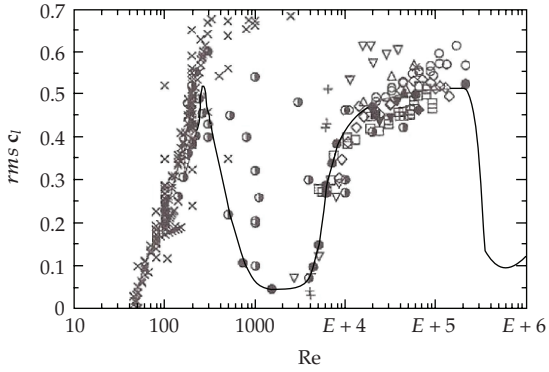

Figure 5: *Lift coefficiente: rms* $\mathbf{c}_l \times$ Re (Norberg [5]). (x: numeric; [•; ⋄; ←; ○; ∇]: experiments)

usual in a subcritical bifurcation, the presence of the two attractors can be detected a little before the critical point $\mathbf{R}_{c2} \cong 190$.

In the range Re > 260 the Strouhal frequency changes weakly with Re and the flow pattern presents a well tuned frequency immersed in a chaotic (turbulent) background. In this range of Reynolds numbers the most conspicuous experimental result is, certainly, the *"lift crisis"* observed by Norberg [5] and briefly commented below.

The *sectional* transverse (lift) force $l(z,t)$ was measured by Norberg [5] in the range 250 < Re < 10 000 and the *rms* of the *lift coefficient* $\mathbf{c}_l(z,t) = l(z,t)/((1/2)\rho U^2 d)$ was plotted as a function of Re, the obtained result being shown in Figure 5. The "lift crisis" corresponds to the sharp drop of *rms* $\mathbf{c}_l$ at Re ≈ 260, reaching a minimum at Re ≈ 1000 of about 20% of the 2D value and there remaining up to Re ≈ 5000, where the value of *rms* $\mathbf{c}_l$ starts a slow recovering.

The behavior is similar to the well known "drag crisis" in the range $10^5 < \mathrm{Re} < 10^6$, although even sharper, and it should be also related to the chaotic (turbulent) flow observed when $\mathrm{Re} > 260$. The main purpose in the present paper is to indicate that the Ginzburg-Landau Equation (GLE) has the potential ability to recover Norberg's "lift crisis" and this point will be addressed next.

3. Ginzburg-Landau Equation in the Defect Chaos Regime

The 2D *unstable mode* $a(t) \cdot \mathbf{e}(\mathbf{x})\exp(i\omega t)$ is triggered by a random perturbation distributed along the cylinder's span and one should expect, as a consequence, a certain phase-lag of this mode in the z-direction: the amplitude a must then change with the span coordinate z, namely, $a = a(z,t)$. The z-dependence of the mode amplitude should modify the 2D Landau's equation by a parcel proportional to a z-derivative of a and observing that there is no preferred z-direction this derivative should be *even* in z: the obvious choice here is to take the *second derivative* $\partial_{zz}a$. This is perhaps the simplest argument to introduce the *Ginzburg-Landau Equation* (GLE),

$$\frac{\partial a}{\partial t} - \sigma a - \gamma(1 + ic_1)\frac{\partial^2 a}{\partial z^2} + \mu(1 - ic_3)|a|^2 a = 0; \quad \{\sigma;\gamma;\mu\} > 0, \tag{3.1}$$

as done by Ginzburg in 1950 in his joint study with Landau on super-conductivity, see Ginzburg [6]. It was introduced then as a *phenomenological model*, namely, as an equation that emulates the overall behavior of an observed phenomenon, and as such has been used in Physics, see Aranson and Kramer [7], to analyze a class of problems related to a *distributed Hopf bifurcation*; the flow around a slender cylinder is just an example of it.

In this context, the GLE was first proposed as a *phenomenological model* by Abarède and Monkewitz [8] and studied by Monkewitz and co-authors in several papers; particularly interesting is the work by Monkewitz et al. [9] where some subtle aspects of the flow are theoretically predicted and confirmed experimentally. These works were restricted, however, to the range $\mathrm{Re} < 160$, within the stable range of the 2D periodic flow, and the purpose here is to extend it to the unstable regime $\mathrm{Re} > \mathbf{R}_{c2} \cong 190$.

Normalizing time, space and amplitude by using $\{t \leftarrow \sigma t;\ z \leftarrow (\sigma/\gamma)^{1/2}z;\ a \leftarrow (\sigma/\mu)^{1/2}a\}$ the same equation (3.1) is obtained with $\sigma = \gamma = \mu = 1$: the behavior of the GLE depends only on the *dispersion coefficients* $\{c_1;c_3\}$ and it is not difficult to show, via Fourier Transform of the perturbed equation, that the 2D solution becomes unstable with respect to 3D perturbation when $c_1 \cdot c_3 > 1$; incidentally, this *stability condition* is usually called the *Benjamin-Feir condition*, in honour of a stability study in *water waves* done by these authors, see Benjamin and Feir [11]. In Figure 6 it is shown the results of a comprehensive numerical study done by Shraiman et al. [10] in the unstable region of the dispersion plane (c_1, c_3). It discloses, at first, two distinct chaotic regimes: one, very mild, called "phase chaos", is characterized by a "turbulence" superposed on the uniform 2D phase and restricted to a small strip on the unstable region $c_1 \cdot c_3 > 1$; the other, very energetic and covering the remaining of the unstable region, called "defect chaos", is related directly to the amplitude size $|a|$: the "*defects*" are the points in time-space plane (z,t) where the amplitude is null and the iso-phases either stop or bifurcate at them, see the plots of the iso-phases in the detached figures in Figure 6. Shraiman et al. [10] also observed a thin strip, coined *bi-chaotic*, close to

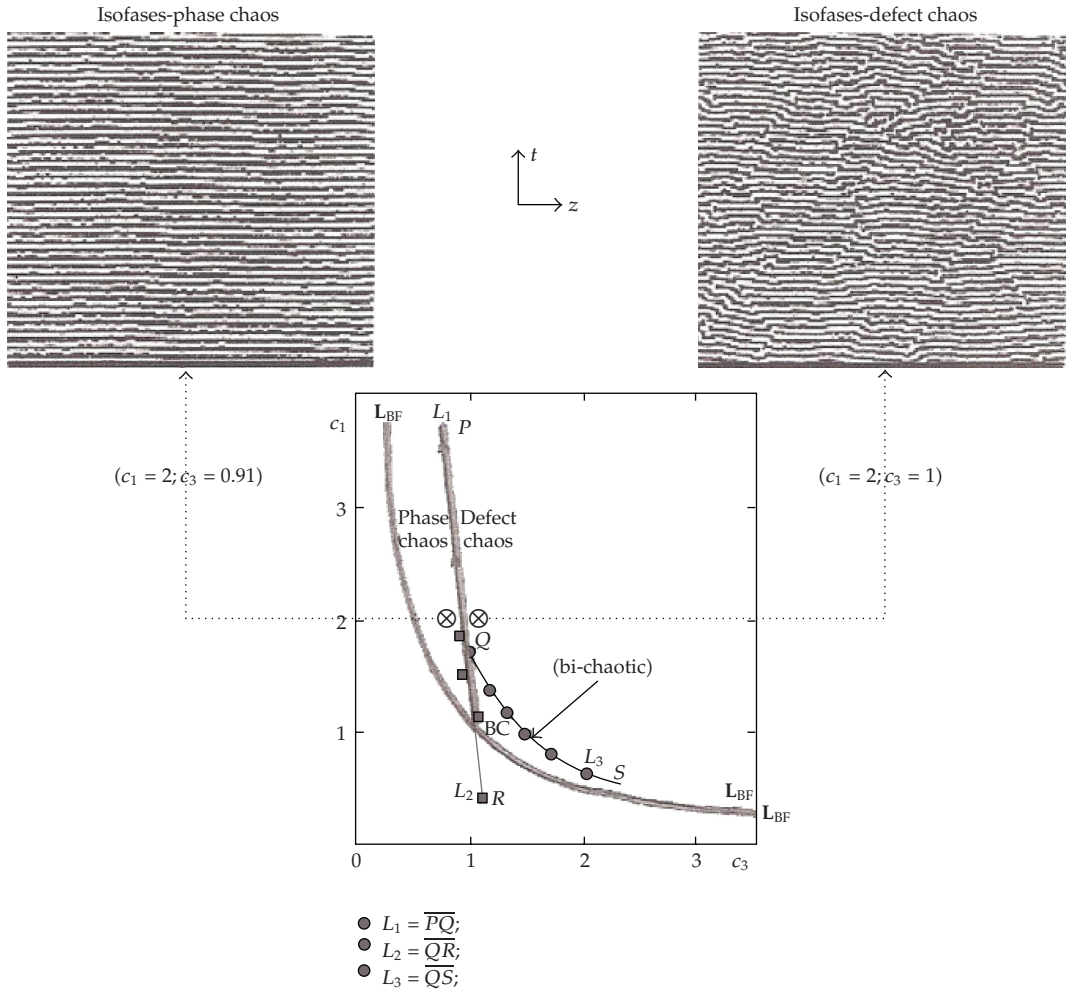

Figure 6: Behavior of GLE in the unstable region ($c_1c_3 > 1$). $\mathbf{L}_{BF}$: $c_1c_3 = 1$. *"Phase chaos"* and *"defect chaos"* regimes and corresponding iso-phases. In the *bi-chaotic* region GLE has two attractors with distinct frequencies. (Source: Shraiman et al. [10].)

the threshold curve $c_1 \cdot c_3 = 1$ and in fact penetrating a little into the stable region $c_1 \cdot c_3 < 1$, where the GLE has two chaotic attractors.

It seems then that the GLE, with recognized predictive ability in the *stable range* (Re < 190 or $c_1 \cdot c_3 < 1$), may be useful also in the *unstable range* (Re > 190 or $c_1 \cdot c_3 > 1$) since, as in the flow problem, it presents a bi-chaotic behavior in the vicinity of the threshold point (Re ≈ 190 or $c_1 \cdot c_3 \approx 1$) and a chaotic one when Re ≫ 190 or $c_1 \cdot c_3 \gg 1$. The difficulty here is first of all operational, since it seems awkward to adjust the parameters of the *phenomenological* GLE to the empirical data of the now chaotic flow, and also conceptual in some sense, once it is understood that GLE can model the problem just in the vicinity of Hopf bifurcation but not far from it, although Monkewitz et al. [9] used GLE to model properly the flow problem at a Re almost three times larger than critical Reynolds $\mathbf{R}_{c1} \cong 46.5$.

However, as seen in the first section, *Landau's equation* can be extended far beyond bifurcation and the GLE can be obtained as an *asymptotic approximation* of the 3D flow related

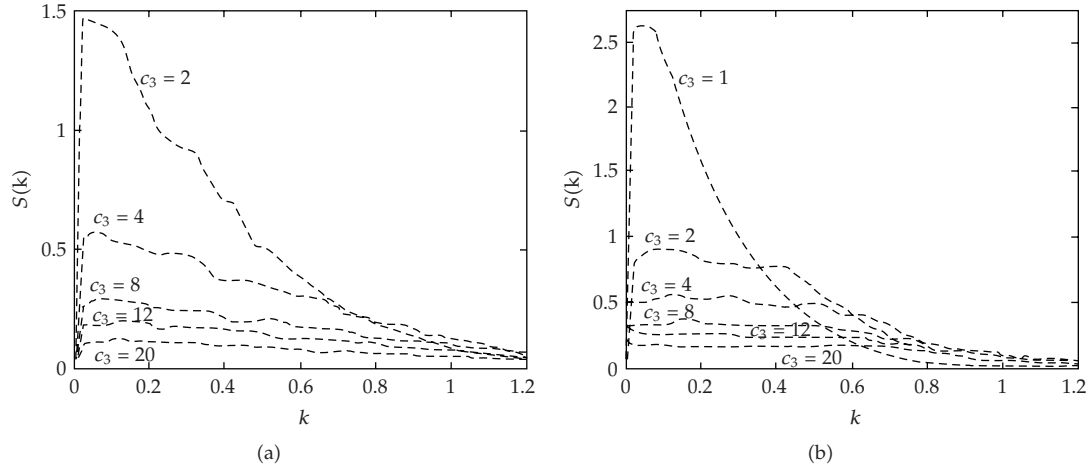

Figure 7: Wavenumber spectrum for several points in the dispersion plane $(c_1; c_3)$. $\sigma = \gamma = \mu = 1$: (a) $c_1 = 1$; (b) $c_1 = 4$. (Burr (2007) —NDF)

to (1.13), allowing one to determine the curve $(c_3(\mathrm{Re}); c_1(\mathrm{Re}))$ representing the flow problem. This computation was not done yet, however, only scarce results are available; meanwhile, it seems interesting to check whether or not GLE has the potential ability to recover the main features of the observed 3D flow. For example, one certainly should expect that the curve $(c_3(\mathrm{Re}); c_1(\mathrm{Re}))$ crosses the *Benjamin-Feir curve* $c_1 \cdot c_3 = 1$ at $\mathrm{Re} \approx 190$, penetrating after the defect chaos regime trough the bi-chaotic region, corresponding to the hysteretic behavior in the range $180 < \mathrm{Re} \leq 260$ observed in Figure 4; as Re rises above 260 the curve $(c_1(\mathrm{Re}); c_2(\mathrm{Re}))$ must go even deeper into the defect chaos regime and, in particular, *Norberg's lift crisis* must be predicted if the GLE approximation is consistent. But the transverse (lift) force is due to the odd harmonics, and so it is proportional to $a(z,t)$: the sharp drop in *rms* $\mathbf{c}_l$ must be related, in the GLE context, to a sharp drop in *rms* $|a(z,t)|$. The purpose here is to discuss this point while revealing some interesting aspects of the GLE in the *defect chaos regime*, that may have an interest in itself.

As in a turbulent flow regime, the chaotic solution in the "defect chaos" regime is characterized by a cascade of length scales k^{-1} limited below by a "Kolmogorov scale" $\left(k_{(\mathrm{kol})}\right)^{-1}$, where the dissipated power, proportional to $\gamma \cdot |\partial_z a|^2$, is of order of the power given by the instability, proportional to $\sigma \cdot |a|^2$; it follows that

$$k_{(\mathrm{kol})} \approx \sqrt{\frac{\sigma}{\gamma}} \quad \text{or} \quad k_{(\mathrm{kol})}\big|_{\sigma=\gamma=1} \approx 1. \tag{3.2}$$

Equation (3.1) was integrated in the region $0 \leq z \leq l = 1000$ in the time interval $18000 \leq t \leq 20000$, using the periodic boundary condition $\{a(0,t) = a(l,t); \partial_z a(0,t) = \partial_z a(l,t)\}$. Figure 7 shows the wavenumber spectrum $S(k)$ of $a(z,t)$ for pairs of values $(c_3; c_1)$ and it is clear that the energy is almost exhausted in the region $k > k_{\mathrm{kol}} \approx 1$. This behavior was observed in all numerical experiments in the grid $\{1 \leq c_3 \leq 20; 1 \leq c_1 \leq 20; c_3 \cdot c_1 > 1\}$.

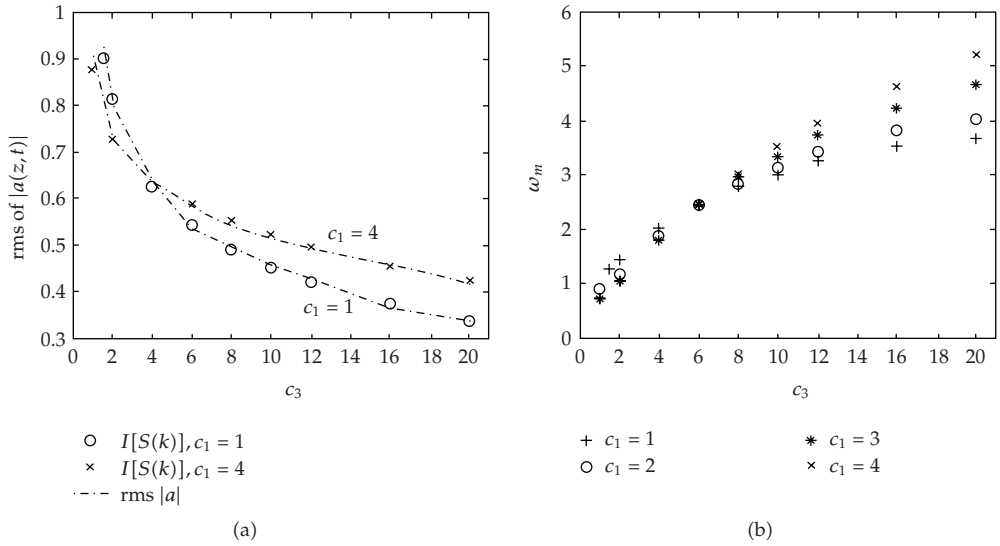

Figure 8: (a) Comparison between (3.3) and *rms* $|a|$; (b) Averaged frequency ω_m. (Burr (2007)—NDF)

The intensity of the response can be also estimated by the wavenumber spectrum integral,

$$I[S(k)] = \int_0^\infty S(k)dk = \frac{1}{l}\int_0^l \left|a(z,t)\right|^2 dz, \tag{3.3}$$

and in Figure 8(a) the values of $I[S(k)]$ and *rms* $|a(z_m,t)|$, $z_m = (1/2)l$, are plotted again for several points in the "dispersion plane" $(c_3; c_1)$. The almost exact agreement between the two plots indicates that the random signal $a(z,t)$ is *weakly stationary*, namely

$$\frac{d}{dt}\int_0^l \left|a(z,t)\right|^2 dz \cong l \cdot \frac{d}{dt}\left(rms\left|a(z_m,t)\right|\right) = 0, \quad \left(z_m = \frac{1}{2}l\right). \tag{3.4}$$

Figure 8(a) shows that the *rms* of $|a(z,t)|$ decreases monotonically with c_3, kept c_1 constant, but when c_3 is constant it increases with c_1, also monotonically in the range $c_3 > 4$. This behavior can be inferred from an identity of the GLE. In fact, if (3.1) is multiplied by a^* and integrated in the interval $0 \le z \le l$, one obtains, after using the periodicity of the boundary conditions and the weak stationary condition (3.4), the identities

$$\begin{aligned} &\text{(i)} \quad -\int_0^l |a|^2 dz + \int_0^l \left|\frac{\partial a}{\partial z}\right|^2 dz + \int_0^l |a|^4 dz = 0; \\ &\text{(ii)} \quad \int_0^l \left(\frac{\partial a}{\partial t}a^* - \frac{\partial a^*}{\partial t}a\right)dz + 2ic_1\int_0^l \left|\frac{\partial a}{\partial z}\right|^2 dz - 2ic_3\int_0^l |a|^4 dz = 0. \end{aligned} \tag{3.5}$$

Now, if $a(z,t) = |a(z,t)| \cdot \exp[i\varphi(z,t)]$ and introducing the average frequency ω_m by the expression

$$\omega_m = \left(\frac{1}{l}\int_0 \frac{\partial\varphi}{\partial t} \cdot |a|^2 dz\right) / I[S(k)], \tag{3.6}$$

one obtains from (3.5)

$$\chi^2 = \frac{m_4}{m_2} = \frac{1 + (\omega_m/c_1)}{1 + (c_3/c_1)}; \qquad m_k = \frac{1}{l}\int_0^l |a|^k dz. \tag{3.7}$$

This relation was obtained under the weak stationary assumption (3.4) and it seems reasonable to assume that the intensity of *rms* $|a(z,t)|$ can be gauged by χ; notice, in particular, that χ is monotonically increasing with c_1 when $\omega_m/c_3 < 1$ and decreasing with c_3 increasing, in accordance to the observed in Figures 8(a), 8(b) for *rms* $|a(z,t)|$. From the relation $\chi \cong rms\ |a(z,t)|$ it follows also the asymptotic relations

$$\begin{aligned} &\text{(i)} \quad \lim_{c_1 \to \infty} \left(rms|a|\right)_{c_3 \cong \mathcal{O}(1)} \cong \mathcal{O}(1); \\ &\text{(ii)} \quad \lim_{c_3 \to \infty} \left(rms|a|\right)_{c_1 \cong \mathcal{O}(1)} \cong \mathcal{O}\left(\sqrt{\frac{c_1 + \omega_m}{c_3}}\right). \end{aligned} \tag{3.8}$$

The expression (ii) in (3.8) can be related to the *Kolmogorov scale* (3.2). In fact, lets recall, first of all, a standard result: by assuming an *harmonic wave solution* $a(z,t) = |a| \cdot \exp[i(k \cdot z + \omega \cdot t)]$ of the GLE (3.1) one obtains the *dispersion relation*,

$$\omega = c_3 \cdot |a|^2 - c_1 \cdot k^2, \quad (\sigma = \gamma = \mu = 1) \tag{3.9}$$

depending on the "dispersion coefficients" $(c_1; c_3)$. For a "random wave" one may take $(rms\ a(z,t))^2$ in the place of $|a|^2$ in (3.9) and if $k = k_{(\mathrm{kol})} \approx 1$ one obtains, with the help of (ii) in (3.8), $\omega \approx \omega_m$, or in short: the averaged frequency defined in (3.6) is the "Kolmogorov frequency scale" of the random signal $a(z,t)$ in the limit $c_3 \to \infty$, kept c_1 constant; in this limit ω_m tends to a bounded value $\omega_\infty(c_1)$, see Figure 8(b). The data of Figure 8(a) confirm, in the limit $\{c_3 \to \infty; c_1 = 1\}$, the asymptotic behavior $rms\ a(z,t) \cong \rho \cdot {c_3}^{-1/2}$ with $\rho \approx (c_1 + \omega_m)^{1/2}$; in reality, $\rho \cong 1.49$ from the data of Figure 8(a) while $(c_1 + \omega_m)^{1/2} \cong 2.17$ from Figure 8(b).

One expects then that $rms\ |a(z,t)|$ diminishes monotonically with increasing c_3, a result confirmed by the direct evaluation of $rms\ |a(z,t)|$ in the dispersion plane (c_3, c_1), see Figure 9; notice that expression (i) in (3.8) is also recovered, a result consistent with the "phase chaos" regime identified in Figure 6.

In the flow problem, the linear dispersion coefficient c_1 is not expected to change too much with Re but c_3, defined by the ratio $(\omega_s - \omega)/\sigma$, see (1.23), apparently does: the difference $(\omega_s - \omega)$ is small but fairly constant while σ appears to drop sharply for Re above 100, the ratio $(\omega_s - \omega)/\sigma = c_3$ becoming very large then: as it was seen, if $c_3 \gg 1$ then $rms\ |a| \ll 1$ and thus $rms\ \mathfrak{c}_l \ll 1$. This result must be confirmed by a more refined numerical solution but it indicates, anyway, the ability of the GLE to predict *Norberg's "lift*

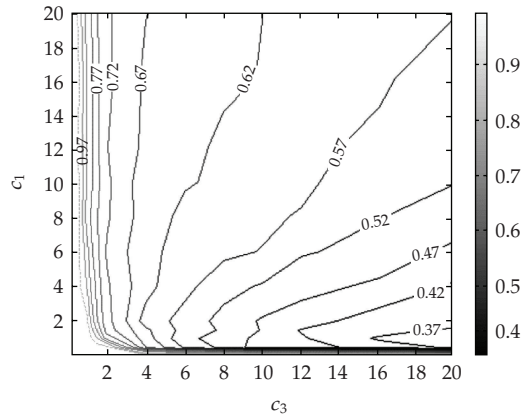

Figure 9: Contour lines of $rms\ a(z,t)$ in the dispersion plane$(c_3; c_1)$. (Burr (2007)—NDF)

crisis." Or, in other words, if the actual curve $(c_3(\mathrm{Re}); c_1(\mathrm{Re}))$ in fact penetrates the unstable range through the bi-chaotic region at $\mathrm{Re} \approx \mathbf{R}_{c2} \cong 190$ and $c_3(\mathrm{Re})$ increases rapidly with Re, then the GLE, together with the asymptotic expansion (1.14), defines in fact a *reduced* Navier-Stokes Equation for the flow around a slender cylinder, the practical importance of it being commented below.

4. Conclusion

In this paper the possibility to solve asymptotically the flow around a slender cylinder using a 2D computation and the Ginzburg-Landau equation to obtain the 3D correction was elaborated, stressing the regime above $\mathrm{Re} \cong 190$, where three dimensionality has a marked influence. Although one must wait more refined numeric results to reach a definitive conclusion, the qualitative behavior of GLE in the range $c_3 \cdot c_1 > 1$ matches very well the most important qualitative features of the flow around a slender cylinder in the range $\mathrm{Re} > 190$; as already discussed in Monkewitz et al. [9] , the matching between both is impressive in the range $\mathrm{Re} < 160$.

A practical problem where the present study may be relevant is related to the *fatigue analysis* of "risers" (vertical ducts) in the offshore oil production systems, essential to assure the safe operation of these systems during its projected life: risers are exposed to ocean currents and oscillate transversally in the elastic modes with natural frequencies close to the flow's Strouhal frequency, the related cyclic stress causing fatigue of the material. The use of a 3D Navier-Stokes code to obtain practical answers is, however, completely out of question in the present stage of development, not only due to computer time needed, but also for the lack of confidence in the numerical results of the enormous discrete system related to it. The *reduced* Navier-Stokes equation, represented by the GLE, opens an opportunity to a feasible and relatively cheap computation: in it, the complex coupling between the *incoming flow* and the *riser's elasticity* can be represented by a coupled set of equations—one of them being the (extended) GLE, the other representing the riser's elastic behavior—both depending only on the space variable along the riser's span, turning the discrete model orders of magnitude smaller. This is the main motivation to study this problem at NDF.

Acknowledgments

The authors acknowledge the financial support from FINEP-CTPetro, FAPESP, PETROBRAS and CNPq.

References

[1] M. van Dyke, *An Album of Fluid Mechanics*, The Parabolic Press, Stanford, Calif, USA, 1982.
[2] D. Barkley, "Linear analysis of the cylinder wake mean flow," *Europhysics Letters*, vol. 75, no. 5, pp. 750–756, 2006.
[3] J. A. P. Aranha, "Weak three dimensionality of a flow around a slender cylinder: the Ginzburg-Landau equation," *Journal of the Brazilian Society of Mechanical Sciences and Engineering*, vol. 26, no. 4, pp. 355–367, 2004.
[4] R. D. Henderson, "Nonlinear dynamics and pattern formation in turbulent wake transition," *The Journal of Fluid Mechanics*, vol. 352, pp. 65–112, 1997.
[5] C. Norberg, "Fluctuating lift on a circular cylinder: review and new measurements," *Journal of Fluids and Structures*, vol. 17, no. 1, pp. 57–96, 2003.
[6] V. L. Ginzburg, *On Superconductivity and Superfluidity*, Nobel Lecture, Springer, Berlin, Germany, 2003.
[7] I. S. Aranson and L. Kramer, "The world of the complex Ginzburg-Landau equation," *Reviews of Modern Physics*, vol. 74, no. 1, pp. 99–143, 2002.
[8] P. Abarède and P. A. Monkewitz, "A model for the formation of oblique shedding and "chevron" patterns in cylinder wake," *Physics of Fluids A*, vol. 4, no. 4, pp. 744–756, 1992.
[9] P. A. Monkewitz, C. H. K. Williamson, and G. D. Miller, "Phase dynamics of Kármán vortices in cylinder wakes," *Physics of Fluids*, vol. 8, no. 1, pp. 91–96, 1996.
[10] B. I. Shraiman, A. Pumir, W. van Saarlos, P. C. Hohenberg, H. Chaté, and M. Holen, "Spatiotemporal chaos in the one-dimensional complex Ginzburg-Landau equation," *Physica D*, vol. 57, no. 3-4, pp. 241–248, 1992.
[11] T. B. Benjamin and J. E. Feir, "The desintegration of wave trains on deep water—part I: theory," *The Journal of Fluid Mechanics*, vol. 27, no. 3, pp. 417–430, 1967.